Changes in timing of seasonal peak photosynthetic activity in northern ecosystems

Running Title: Shifting timing of peak plant photosynthesis

Taejin Park[1,*], Chi Chen[1], Marc Macias-Fauria[2], Hans Tømmervik[3], Sungho Choi[4], Alexander Winkler[5,6], Uma S. Bhatt[7], Donald A. Walker[8], Shilong Piao[9], Victor Brovkin[5], Ramakrishna R. Nemani[10], Ranga B. Myneni[1]

[1]Department of Earth and Environment, Boston University, Boston MA 02215, USA

[2]School of Geography and the Environment, University of Oxford, Oxford OX1 3QY, UK

[3]Norwegian Institute for Nature Research, FRAM – High North Research Centre for Climate and the Environment, NO-9296 Tromsø, Norway

[4]Rhombus Power Inc., NASA Ames Research Park, Moffett Field, CA 94035, USA

[5]Max-Planck-Institute for Meteorology, Bundesstrasse 53, 20146 Hamburg, Germany

[6]International Max-Planck Research School for Earth System Modeling, Bundesstrasse 53, 20146 Hamburg, Germany

[7]Geophysical Institute, University of Alaska Fairbanks, Fairbanks, AK 99775-7320, USA

[8]Institute of Arctic Biology, University of Alaska, Fairbanks, AK 99775-7000, USA

[9]College of Urban and Environmental Sciences, Peking University, Beijing 100871, China

[10]NASA Ames Research Center, Moffett Field, CA 94035, USA

*Corresponding author. Email: parktj@bu.edu; Phone: +1 617 893 1988

Key words (6 to 10): photosynthetic seasonality, climate constraint, law of minimum, gross primary productivity, carbon cycle, climate change, remote sensing, eddy-covariance, earth system model

ABSTACT

Seasonality in photosynthetic activity is a critical component of seasonal carbon, water and energy cycles in the Earth system. This characteristic is a consequence of plant's adaptive evolutionary processes to a given set of environmental conditions. Changing climate in northern lands (>30°N) alters the state of climatic constraints on plant growth, and therefore, changes in the seasonality and carbon accumulation are anticipated. However, how photosynthetic seasonality evolved to its current state, and what role climatic constraints and their variability played in this process and ultimately in carbon cycle is still poorly understood due to its complexity. Here, we take the 'laws of minimum' as a basis and introduce a new framework where the timing (Day of Year) of peak photosynthetic activity (DOY_{Pmax}) acts as a proxy for plant's adaptive state to climatic constraints on its growth. Our analyses confirm that spatial variations in DOY_{Pmax} reflect spatial gradients in climatic constraints as well as seasonal maximum and total productivity. We find a widespread warming-induced advance in DOY_{Pmax} (-1.66 ± 0.30 days decade^{-1}, $P < 0.001$) across northern lands, indicating a spatio-temporal dynamism of climatic constraints to plant growth. We show that the observed changes in DOY_{Pmax} are associated with an increase in total gross primary productivity through enhanced carbon assimilation early in the growing season, which leads to an earlier phase shift in land-atmosphere carbon fluxes and an increase in their amplitude. Such changes are expected to continue in the future based on our analysis of Earth System Model (ESM) projections. Our study provides a simplified, yet realistic framework based on first principles for the complex mechanisms by which various climatic factors constrain plant growth in northern ecosystems.

INTRODUCTION

Warming is generally thought to ease climate constraint on photosynthetic activity of vegetation in northern lands. Indeed, recent growing season studies based on ground observation (Parmesan & Yohe, 2003), eddy covariance (Richardson et al., 2010; Keenan et al., 2014), remote sensing (Xu et al., 2013; Park et al., 2016), and model simulation (Duveneck & Thompson, 2017) have concordantly indicated that the growing season duration for northern terrestrial vegetation has significantly extended over the past decades due to both an earlier start and delayed termination. This prolonged growing season over northern land drives a longer carbon assimilation period due to the relaxation of low temperature limits on metabolism, and in turn increased productivity and carbon uptake have been observed (Xu et al., 2013; Forkel el al., 2016). However, longer and warmer growing seasons also promote environmental conditions that favor surface drying, and thus intensified summer droughts, tree mortality, and wildfires have resulted in summer productivity decline (Peng et al., 2011; Barichivich et al., 2014; D'Orangeville et al., 2018). These consequential dynamics are highly variable in space and over time, and indicate a complex interaction of multiple climate constraints on plant growth and its dynamism (Nemani et al., 2003; Garonna et al., 2018; Reich et al., 2018). To accurately project the response of northern vegetation to future climate, we need to better understand how climate-vegetation interaction has evolved to its current state, and what role climatic constraints and their variability played in this process.

Photosynthetic seasonality is an integrated outcome of how plants adapt to seasonal variations in climatic constraints (Chuine & Beaubien, 2001; Jolly et al., 2005; Eagleson, 2005; Garonna et al., 2018), and is thus a critical indicator of vegetation-climate interaction. For instance, gross

primary productivity (GPP) tracks the seasonal course of temperature in northern high-latitude ecosystems, while the synchrony between GPP and temperature is gradually lost southwards towards warmer and drier environments (see Figure 1 in Rotenberg & Yakir, 2010). The laws of minimum (Sprengel, 1828; Liebig, 1841; Blackman, 1905) explain these shifts in GPP with respect to varying climatic conditions (Eagleson, 2005). The laws state that although photosynthetic activity is controlled by multiple factors (e.g., radiation, temperature, water availability, etc.), the prevailing rate is set by the most deficient of these factors (Sprengel, 1828; Liebig, 1841; Blackman, 1905). This suggests that the timing (Day of Year) of peak photosynthetic rate (DOY_{Pmax}) during the seasonal course corresponds to the period when the primary climatic factor controlling plant growth is least limiting. This simple yet intuitive indicator has an indispensable role not only indicating the timing and magnitude of resource availability (i.e., constraint) but also the capacity of terrestrial ecosystem productivity (Xia et al., 2015; Zhou et al., 2017). Ongoing climate change in the north is expected to alter the state of climatic constraints on plant growth, and therefore, changes in DOY_{Pmax} and productivity. Previous studies have observed trends toward an earlier peak of the growing season (Buitenwerf et al., 2015; Gonsamo et al., 2018). However, the underlying mechanisms for spatially varying relations between its changes and implications on seasonal total productivity and carbon cycle are still largely unknown.

In this study, we take the 'laws of minimum' as a basis and introduce a new framework where the timing of peak photosynthetic activity (DOY_{Pmax}) acts as a proxy for plant's adaptive state to climatic constraints on its growth. Two basic principles formulate this new framework (Figure 1). First, under non-limiting climatic conditions, DOY_{Pmax} will show a tendency to coincide with

97 the period of seasonal peak radiation load so as to result in maximum photosynthetic capacity
98 conditions (Eagleson, 2005; Bauerle et al., 2012) (Case 1 in Figure 1). Second, if a climatic
99 factor acts as the primary constraint to photosynthetic activity, DOY_{Pmax} should shift towards the
100 period in the seasonal course at which that limiting resource is more available (Eagleson, 2005;
101 Rotenberg & Yakir, 2010) (Cases 2–4 in Figure 1). In this framework, the timings of peak GPP
102 (DOY_{Pmax}) and three climatic factors including temperature (DOY_{Tmax}), radiation (DOY_{Rmax}),
103 and water availability (DOY_{Wmax}) serve as key proxies for climate resource availability. We only
104 introduce these three abiotic controls of GPP because it is widely known that they interact to
105 primarily impose complex and varying limitations on vegetation activity (Nemani et al., 2003).
106 Thanks to reduced water losses during the cold season over northern terrestrial ecosystems and
107 thermal inertia, a sequential order of the timings of peak climatic factors ($DOY_{Wmax} < DOY_{Rmax}$
108 $< DOY_{Tmax}$) simplifies our framework (Figure S1). In other words, this suggests that positioning
109 of DOY_{Pmax} with respect to DOY_{Rmax} ($\delta DOY_{P,R} = DOY_{Pmax} - DOY_{Rmax}$) can indicate the primary
110 climatic constraint on ecosystems, i.e., water ($\delta DOY_{P,R} < 0$) or temperature ($\delta DOY_{P,R} > 0$).
111 $\delta DOY_{P,T}$ defined as $DOY_{Pmax} - DOY_{Tmax}$ is additionally introduced to subdivide dominant
112 temperature constrained northern ecosystems.

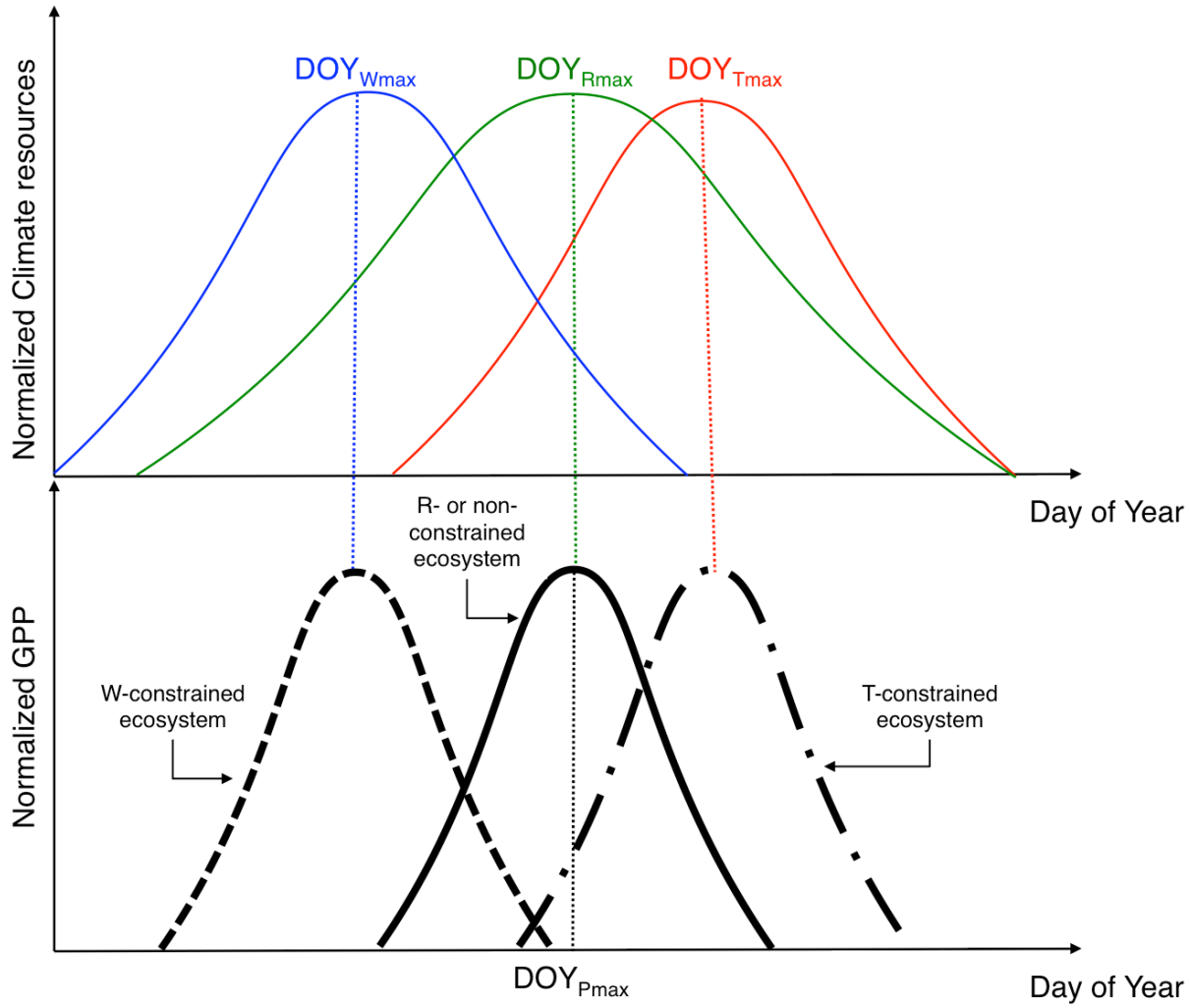

113

114 **Figure 1.** Conceptual illustration of the proposed DOY_{Pmax} framework. Seasonal cycle of
115 temperature (T, red), radiation (R, green), water availability (W, blue) and GPP (P, black) over
116 common northern terrestrial ecosystems. Vertical lines indicate when each variable reaches a
117 maximum state. DOY_{Pmax}, DOY_{Tmax}, DOY_{Rmax}, and DOY_{Wmax} stand for the day of year when
118 GPP, temperature, radiation and precipitation reach respective maximum state during each
119 seasonal course of the year. Four idealized cases are shown to demonstrate how photosynthetic
120 seasonality of the ecosystem under given climate constraint differs from each other: non- (solid
121 line, Case 1), temperature- (dotdash line, Case 2), water- (longdash line, Case 3), and radiation-
122 (solid line, Case 4) constrained ecosystems.

123 Our primary objectives of this study are two-fold: 1) to examine the proposed framework using
124 independent multiple datasets and understand how northern vegetation seasonality has been
125 characterized; 2) to investigate changes in DOY_{Pmax} and its impact on seasonal total productivity
126 and carbon cycle. To accomplish the objectives, we apply the proposed framework to GPP
127 dynamics from the satellite observed vegetation photosynthetic activity to evaluate its validity
128 and changes in DOY_{Pmax}. Two independent sources of vegetation productivity (tower measured
129 GPP and satellite driven Sun-Induced Fluorescence, SIF) are used to further test the framework.
130 We use the atmospheric CO_2 observations at Point Barrow (71.3° N, 156.6° W) and two state-of-
131 the-art CO_2 inversion estimates to investigate the potential impact of shifting DOY_{Pmax} on
132 terrestrial ecosystem carbon cycle. A set of Earth System Models (ESMs) is additionally
133 introduced to evaluate the reproducibility of the observed DOY_{Pmax} changes and their
134 consequences under historical and future climate scenarios.
135
136 **MATERIALS AND METHODS**
137 ***Study area and bioclimatic zones***
138 Only non-agricultural vegetation over north of 30°N is considered in this study to minimize
139 human-induced influence. Three bioclimatic zones including arctic, boreal and temperate regions
140 were used to present outcomes of this study. To discriminate the bioclimatic zones, we combined
141 a terrestrial ecoregion scheme (Olson et al., 2001) of the World Wildlife Fund (WWF) and the
142 Moderate Resolution Imaging Spectroradiometer (MODIS) International Geosphere-Biosphere
143 Programme (IGBP) land cover data (Friedl et al., 2010) (Collection 5.1). We first used MODIS
144 IGBP to keep only non-agricultural vegetation classes (Class 1-10, and 16). Then, based on the
145 WWF's eco-region scheme, tundra and boreal forests/taiga ecoregions were assigned into the

146 arctic and boreal bioclimatic zones, respectively. Temperate broadleaf and mixed forests,
147 temperate coniferous forests, temperate grasslands, savannas, and shrublands were identified as
148 the temperate bioclimatic zone. We further excluded the pixels containing more than 25% of
149 cropland based on the International Institute for Applied Systems Analysis (IIASA) cropland
150 fraction data (Fritz et al., 2015).
151
152 ***Data and methods***
153 ***Multi-scale GPP and its proxy: satellite and tower measurements***
154 In this study, we mainly used 17-year (2000 to 2016) time series of GPP data from the MODIS
155 aboard NASA's Terra satellite (Running et al., 2015) to examine the framework and to
156 investigate DOY_{Pmax} change in northern lands. The latest version (Collection 6) of MODIS GPP
157 with 8-day temporal composite was spatially aggregated into 0.05 degree grid. Its high temporal
158 frequency is advantageous to capture the seasonal variation of photosynthetic activity. MODIS
159 GPP is based on a production efficiency model that uses the product of the absorbed
160 photosynthetically active radiation by vegetation and a light use efficiency factor. The quality of
161 MODIS GPP data sets has been comprehensively evaluated against multiple eddy-covariance
162 tower measurements of GPP and through inter-comparisons with other GPP products (Zhao et
163 al., 2005; Heinsch et al., 2006).
164
165 We additionally introduced satellite-driven SIF and eddy-covariance based GPP data to verify
166 our framework and results from MODIS GPP. The SIF is retrieved near the λ = 740 nm far-red
167 peak in chlorophyll fluorescence emission from the Global Ozone Monitoring Experiment-2
168 (GOME-2) instrument onboard Eumetsat's MetOp-A satellite. The monthly SIF record (version

27, level 3) covering 2007 to 2016 was used in this study (Joiner et al., 2016). SIF is an electromagnetic emission in the 650-800 nm range originating from plant photosynthetic machinery, and it is theoretically linearly correlated with the electron transport rate of photosynthetic activity (Zhang et al., 2014).

The eddy-covariance tower measurements from the FLUXNET2015 database (tier 1, Pastorello et al., 2017) were used in this study. FLUXNET is a global network of micrometeorological tower sites that use eddy covariance methods to measure the exchanges of carbon, water, and energy between terrestrial ecosystems and the atmosphere (Baldocchi et al., 2001). We used GPP estimates based on the flux partitioning approach proposed by Lasslop et al. (2010). A total of 92 sites (those with more than 3 site-year measurements) were selected for the evaluation of our DOY_{Pmax} framework spanning a large climatic and biome gradient (Figure S2a).

Multi-scale climate data

We used daily climate datasets provided by Global Modeling and Assimilation Office (GMAO) Reanalysis of NASA (Gelaro et al., 2017). The current version of GMAO is an hourly time step dataset generated by Goddard Earth Observing System-5 (GEOS-5) data assimilation system. We aggregated the native hourly data into the daily scale to retrieve pixel-wise phases of climate variables. Surface air temperature and down-welling photosynthetically active radiation were employed in this analysis. Daily climate datasets were used to characterize DOY_{Tmax} and DOY_{Rmax}. We also obtained potential evapotranspiration (PET) and actual evapotranspiration (AET) to quantify water availability on plant growth by calculating a ratio of AET to PET (RAP) (Prentice et al., 1992). Both AET and PET were obtained by Global Land Data Assimilation

Systems (GLDAS, Version 2.1) (Rodell et al., 2004). We characterized summer climate using mean temperature and RAP during June–August for investigating how DOY_{Pmax} positioning varies as functions of climate constraints, i.e., temperature and water availability. For the tower measured GPP, the ancillary microclimate datasets including air temperature and incoming radiation (Photosynthetic photon flux density, PPFD) simultaneously measured with GPP were additionally obtained.

Earth System Model simulated historical and future GPP

We also introduced a set of the most recent climate-carbon simulations of ESMs contributing to the fifth phase of the Coupled Model Intercomparison Project, CMIP5 (Taylor et al., 2012). Seven ESMs, which are available at CMIP5 archive, were used in this study: NorESM1-M, MIROC-ESM, CanESM2, HadGEM2-ES, IPSL-CM5A-MR, MPI-ESM-MR and CCSM4. The datasets provided monthly GPP output (1980 to 2099) for simulations of both Historical and Representative Concentration Pathway (RCP) 4.5 (Thomson et al., 2011). Data from the Historical and RCP4.5 scenario periods were combined to generate continuous variable fields from 1980 to 2099. All model outputs were processed at the native spatial resolutions and aggregated into regional scales (i.e., arctic, boreal, and temperate regions) for trend and correlation estimates.

Timings of peak seasonal photosynthetic activity and climate

We extracted three metrics indicating a maximal state of seasonal photosynthetic activity (DOY_{Pmax}), radiation (DOY_{Rmax}), and temperature (DOY_{Tmax}) at two different scales: site and regional scale. For both scales, to reduce noise and maintain a distinct seasonal feature of GPP

(or SIF) and climate datasets, the singular spectrum analysis was first implemented at yearly basis (Vautard et al., 1992). The singular spectrum analysis is a nonparametric approach that does not need a priori specification of models of time series, thus it is data-adaptive. It first decomposes a time series into oscillatory components and noises according to the singular value decomposition, thereafter reconstructs specific components (i.e., seasonal signal) from the original time series. This non-parametric approach has been widely used to reconstruct the time series of GPP and other environmental variables by reducing their noise components (Keenan et al., 2014; Zhou et al., 2017). Time series of GPP and meteorological datasets were used to retrieve DOY_{Pmax}, DOY_{Rmax}, and DOY_{Tmax} on a yearly basis. Note that multi-year averaged daily GPP, radiation, and temperature time series were used for FLUXNET retrievals. For the case of monthly data (SIF and CMIP5 GPP), we assigned middle of the month as the day of the year for each month and then implemented the same procedures used in MODIS and FLUXNET. Finally, $\delta DOY_{P,R}$ (i.e., $DOY_{Pmax} - DOY_{Rmax}$) and $\delta DOY_{P,T}$ (i.e., $DOY_{Pmax} - DOY_{Tmax}$) were also calculated. We additionally retrieved pixel-wise growing season length from MODIS GPP by applying a fixed threshold, i.e., 10% of the multi-year average maximum GPP (Zhou et al., 2017).

Atmospheric CO_2 concentration and fluxes: zero-crossing date and seasonal amplitude

Daily atmospheric CO_2 concentration at Point Barrow (71.3° N, 156.6° W) was obtained from the in situ measurement dataset provided by the National Oceanic and Atmospheric Administration / Earth System Research Laboratory (NOAA / ESRL). The spring downward CO_2 zero-crossing date ($DOY_{Zero\text{-}Crossing}$) was extracted by following the approach described in Piao et al. (2008). We first detrended the interannual trend in the atmospheric CO_2 concentration

238 with a quadratic polynomial curve, four harmonics in the seasonal function, and time-filtered
239 residuals. We then used the harmonics plus the residuals (detrended CO_2 seasonal cycle) to
240 define the downward CO_2 $DOY_{Zero\text{-}Crossing}$ as the day on which the detrended curve crossed the
241 zero line from positive to negative. All aforementioned processes were achieved by the use of the
242 standard package CCGCRV from NOAA/ESRL (Thoning et al., 1989). We used $DOY_{Zero\text{-}Crossing}$
243 as an indicator of proximal DOY_{Pmax} for three reasons, although $DOY_{Zero\text{-}Crossing}$ is not an
244 accurate term of peak photosynthesis timing. First, seasonal trajectory of GPP strongly governs
245 changes in net biome productivity seasonality and its trend (Ito et al., 2016; Forkel et al., 2016).
246 Second, $DOY_{Zero\text{-}Crossing}$ can be determined more accurately and it is roughly corresponding to the
247 time of maximum carbon uptake by the biosphere (Ito et al., 2016). Third, a relative change in
248 the phase of the cycle identified at one point (e.g. $DOY_{Zero\text{-}Crossing}$) will be matched by relative
249 phase changes at all other points since the shape of the seasonal cycle does not change
250 significantly (Barichivich et al., 2012). We further extracted the seasonal cycle amplitude (SCA)
251 because its changes reflect vegetation GPP driven changes in net carbon uptake (Forkel et al.,
252 2016).
253
254 We additionally used two gridded carbon fluxes from atmospheric CO_2 inversion products: the
255 Copernicus Atmosphere Monitoring Service (Chevallier et al., 2010) (CAMS, version v15r2,
256 1979-2015) and the Jena CarboScope (Rödenbeck et al., 2003) (JENA, version s81_v3.8, 1981-
257 2015). Atmospheric CO_2 inversions estimate net carbon exchange fluxes between surface and
258 atmosphere by utilizing CO_2 concentrations at measurement sites, combined with an atmospheric
259 transport model and prior information on fossil fuel carbon emissions and carbon exchange
260 between the atmosphere and land (and ocean). We used daily mean net flux estimates on a
261 spatial resolution of 3.75° latitude and 5° longitude (JENA) and 1.875° latitude and 3.75°

longitude (CAMS) over the vegetated land surface. Both products were firstly aggregated into regional scales then $DOY_{Zero\text{-}Crossing}$ and SCA of carbon fluxes were respectively extracted. Note that the flux amplitude is indirectly related to the amplitude in the atmospheric CO_2 concentration, as the atmospheric concentration is roughly the integral of the fluxes (Welp et al., 2016).

Analytical approach

Based on the extracted MODIS DOY_{Pmax}, we first tested the validity of framework by relating it to summer climate conditions (i.e., temperature and water availability). The first principle we formulated for the framework justifies using summer season as a period when the primary climate constraint dictates vegetation photosynthetic seasonality, and therefore, DOY_{Pmax}. Both seasonal total (GPP_{Total}) and maximum GPP (GPP_{Pmax}) were calculated to investigate the spatial and temporal relations between DOY_{Pmax} and vegetation productivity. In order to capture the seasonal distribution of GPP with a simple metric, we evaluated the ratio (GPP_{Ratio}) of total GPP during the first half (January 1st to the long-term mean DOY_{Pmax}) to that of the whole year. Additionally, the length of growing season together with GPP_{Pmax} was considered to explain the observed pattern between DOY_{Pmax} and GPP_{Total} (e.g., Xia et al., 2015). All explored relationships were explained as functions of $\delta DOY_{P,R}$ and $\delta DOY_{P,T}$. Independent eddy-covariance tower GPP and GOME-2 SIF based retrievals were used for further testing of the framework. Note that we limited the use of these independent data only for verifying the framework and not the change analysis because of limited temporal frequency and coverage of the data.

For the time series analysis, all trends in time series were computed as the slope of linear trends based on ordinary least squares regression. The significance of the trend was computed by using the non-parametric Mann-Kendall trend test. The standard error of the trend slope is also reported. We estimated the decadal trend based on the 5-year moving average approach to reduce the potential impact of first, last and outlier points. The Kendall's rank correlation coefficient (r) was used to measure the ordinal association between given two quantities. To understand how warming-induced DOY_{Pmax} shift has characterized northern land vegetation productivity, we investigated changes in temperature, DOY_{Pmax}, GPP_{Total}, and GPP_{Ratio}. This analysis was applied to both MODIS and ESMs based retrievals. A trend in $DOY_{zero\text{-}crossing}$ of three CO_2 data was respectively computed and correlation analysis between annual variations in $DOY_{zero\text{-}crossing}$ and SCA was performed.

RESULTS

Spatial pattern of MODIS DOY_{Pmax} and its determinants

A distinct spatial gradient exists in DOY_{Pmax} and in its positioning with respect to the seasonal course of radiation and temperature (Figures 2a and Figure S2a,b). Overall, DOY_{Pmax} in arctic ecosystems is more closely aligned with DOY_{Tmax} ($\delta DOY_{P,T}$ = −9.3 ± 5.5 days, mean ± 1 s.d.) than DOY_{Rmax} ($\delta DOY_{P,R}$ = 29.1 ± 8.5 days), while in the boreal ecosystems it shows a much closer alignment with peak radiation levels ($\delta DOY_{P,T}$ = −13.3 ± 5.4 days, $\delta DOY_{P,R}$ = 12.9 ± 10.5 days). In the temperate regions, $\delta DOY_{P,R}$ is negative (−9.5 ± 27.0 days), i.e., DOY_{Pmax} precedes DOY_{Rmax}. Temperature and water availability (i.e., RAP) limiting photosynthetic activity elucidate the observed regional variations in DOY_{Pmax} positioning. Every 1 °C increase in temperature results in a $\delta DOY_{P,R}$ change of −5.7 ± 0.1 days (slope ± SE, Figure 2b). In regions

with negative $\delta DOY_{P,R}$, every 1% decrease in water availability results in a $\delta DOY_{P,R}$ change of -1.8 ± 0.1 days (Figure 2c). These results follow the two tenets of our framework, as outlined earlier complying with the laws of minimum (Sprengel, 1828; Liebig, 1841; Blackman, 1905). This suggests that the use of DOY_{Pmax} and its positioning in relation to DOY_{Rmax} and DOY_{Tmax} represents a feasible approach to assess plant's adaptive state to climatic constraints.

Climate constraints, MODIS DOY_{Pmax} and seasonal vegetation productivity

Emerging climatic constraints to plant growth are directly linked to changes in both GPP_{Total} (Figure 2d) and GPP_{Pmax} (Figure S2c). Regions with large GPP_{Pmax} are associated with tight synchrony between DOY_{Pmax} and $DOY_{Rmax,}$ i.e., both energy and water accessibility are least limiting (Bauerle et al., 2012). Ecosystems under either temperature- ($\delta DOY_{P,R} > 0$) or water-limited ($\delta DOY_{P,R} < 0$) environments show lower photosynthetic capacity by complying the general idea of climatic constraints to plant growth. Such interaction limiting photosynthetic activity is also tightly associated with growing season duration (Figure S2d). It is interesting to note that in areas with the largest GPP_{Total} (~ 1.07 kg C m^{-2}), DOY_{Pmax} slightly precedes DOY_{Rmax} ($\delta DOY_{P,R} \approx -7$ days) because of a joint control by growing season length and GPP_{Pmax} (Xia et al., 2015). The longest growing season duration (~ 6.5 months) is found when $\delta DOY_{P,R}$ is approximately equal to −17 days. This is known as 'phenological trade-off', i.e., a longer growing season imposed by warmer environment may result in a higher GPP_{Total}, but warmer and drier summers may suppress GPP_{Pmax}, potentially offsetting the increased amount of GPP_{Total} (Duveneck & Thompson, 2017).

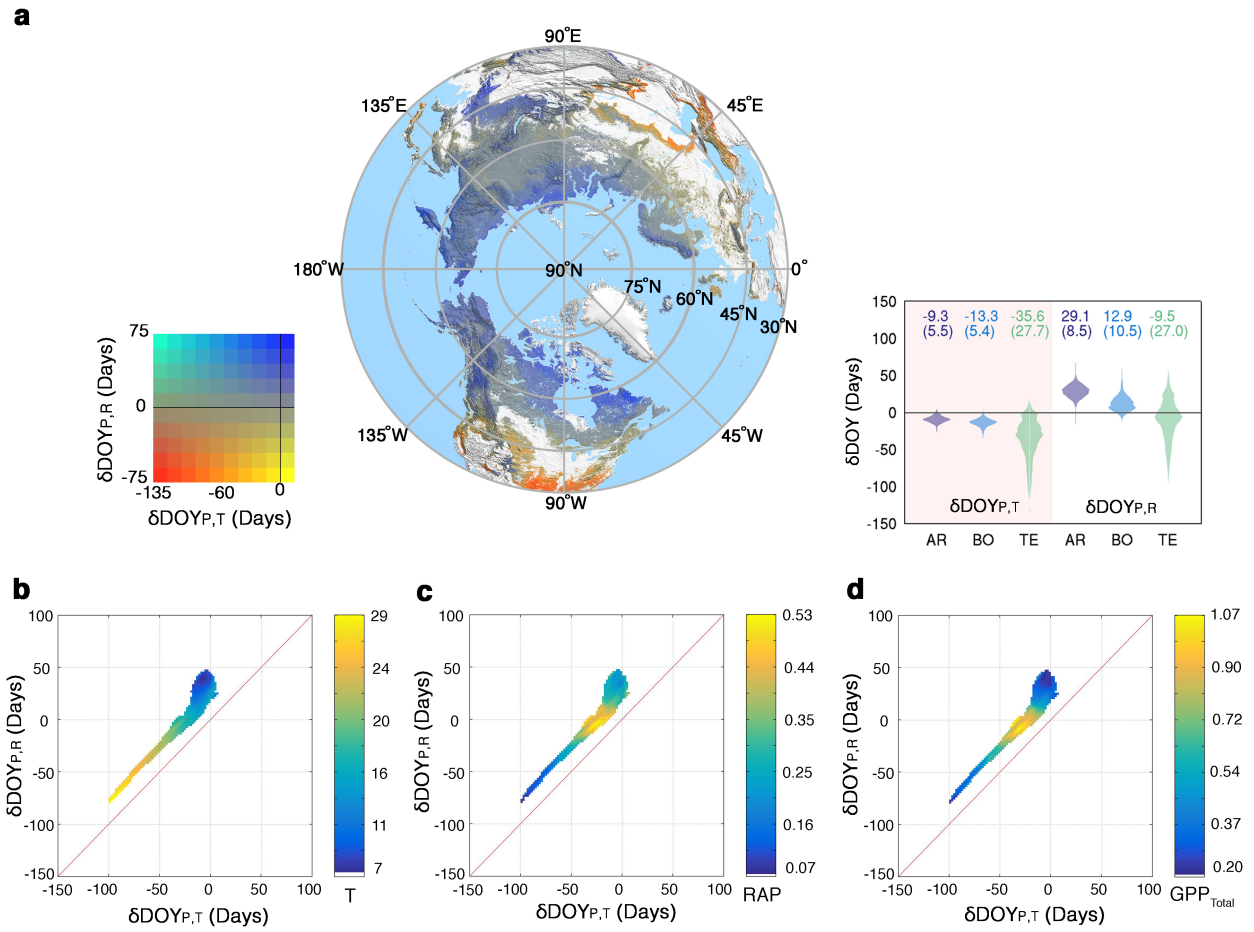

330

331 **Figure 2.** Relative positioning of peak photosynthetic activity timing with respect to the seasonal
332 course of temperature and radiation, and its relation to climatic constraints and productivity. **a,**
333 Geographical distribution of $\delta DOY_{P,T}$ ($DOY_{Pmax} - DOY_{Tmax}$) and $\delta DOY_{P,R}$ ($DOY_{Pmax} -$
334 DOY_{Rmax}) for northern ecosystems. Regional distribution of $\delta DOY_{P,T}$ and $\delta DOY_{P,R}$ over Arctic
335 (AR), Boreal (BO) and Temperate (TE) regions is given in the inset violin plot with mean and 1
336 SD (bracket). **b,** Positioning of DOY_{Pmax} seen as the relation between $\delta DOY_{P,R}$ and $\delta DOY_{P,T}$,
337 with respect to temperature (°C). **c,** Same as **b** but for water availability (i.e., RAP). **d,** Same as **b**
338 but for GPP_{Total} (kg C m^{-2}). MODIS-derived outcomes are used for these panels.

339

340 ***Confirmed patterns from two independent data: SIF and Eddy-Covariance tower GPP***

341 Flux tower-measured GPP data from the eddy-covariance network and GOME-2 SIF confirm the
342 above patterns observed in MODIS GPP products, thus lending further support for the proposed
343 DOY_{Pmax} framework (Figures 3 and Figure S3).

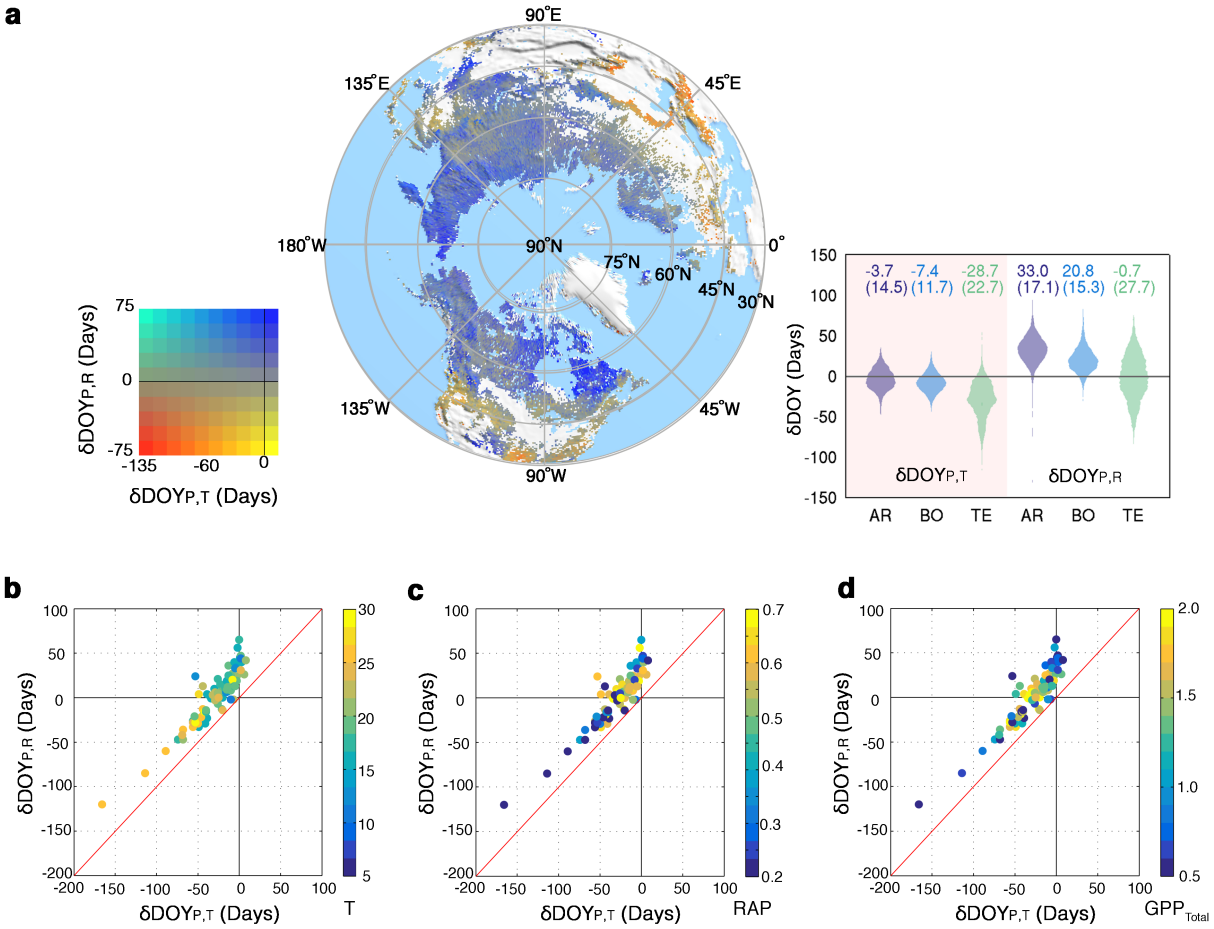

Figure 3. a, Same as Figure 2a but for the independent satellite Sun-Induced Fluorescence (SIF). **b-d,** Same as Figure 2b-d but for the eddy covariance tower measurement. Total 92 FLUXNET sites (Figure S2a) were used and each dot represents a single site.

Changes in MODIS DOY$_{Pmax}$ during last 17 years

Trend analyses reveal a widespread shift in MODIS DOY$_{Pmax}$ towards earlier in the growing season dominating across 60.6 % of the northern vegetated area during last 17 years, and 32.8 % of the area showing a significant negative trend ($P < 0.1$, Figure 4). These changes are seen across all three bioclimatic zones, i.e., 31.9 %, 38.7 % and 26.8 % of the arctic, boreal and temperate regions, respectively. At a hemispheric scale, we detected a significant trend towards an earlier peak photosynthetic rate of −1.66 ± 0.30 days decade^{-1} (slope ± s.e., $P < 0.001$) (Figure 5a), with regionally varying degree of advancing trends: a steeper change in the boreal region (−2.46 ± 0.47 days decade^{-1}, $P < 0.001$) relative to the temperate (−1.07 ± 0.26 days decade^{-1}, $P < 0.001$) and arctic regions (−1.09 ± 0.29 days decade^{-1}, $P < 0.001$). These changes are mostly associated with warming in the lands north of 30°N (Figure 4b and Figure 5b). The sensitivity of DOY$_{Pmax}$ to warming was detected to be greater in the temperate (−4.27 ± 1.50 days °C^{-1}, $P < 0.001$) than in the arctic (−3.88 ± 1.29 days °C^{-1}, $P < 0.001$) and boreal (−3.91 ± 1.02 days °C^{-1}, $P < 0.001$) regions. Note that regionally varying warming rates (TE < AR < BO) lead to a different order of trend and sensitivity estimates. These changes in DOY$_{Pmax}$ are interpreted as shifts in δDOY$_{P,R}$ across the arctic (−1.98 ± 7.30 days, mean ± SD, *t*-test, $P < 0.001$), boreal (−3.21 ± 5.83 days, $P < 0.001$) and temperate (−1.28 ± 12.76 days, $P < 0.001$) regions (Figure S4a,b). We find that the observed shift in DOY$_{Pmax}$ is mainly responsible for the changes in δDOY$_{P,R}$ (and δDOY$_{P,T}$) because of relatively stable DOY$_{Rmax}$ and DOY$_{Tmax}$ changes (Figure S4 and Table S1). According to the principles in our framework, the shifts resulting a newly established photosynthetic seasonality with respect to seasonal climate factors imply changes in vegetation response to varying climatic constraints, i.e., reduced relative importance of thermal

constraint in the arctic and boreal vegetation while enhanced role of water availability in the temperate regions (Garonna et al., 2018; Piao et al., 2017; Fu et al., 2015; Allen et al., 2010) (Figures 2b,c and 5a). Note that some regions transitioning from positive to negative $\delta DOY_{P,R}$ might experience a critical tipping point where the ecosystems moves from temperature- towards water-limited ecosystems (Figure S5).

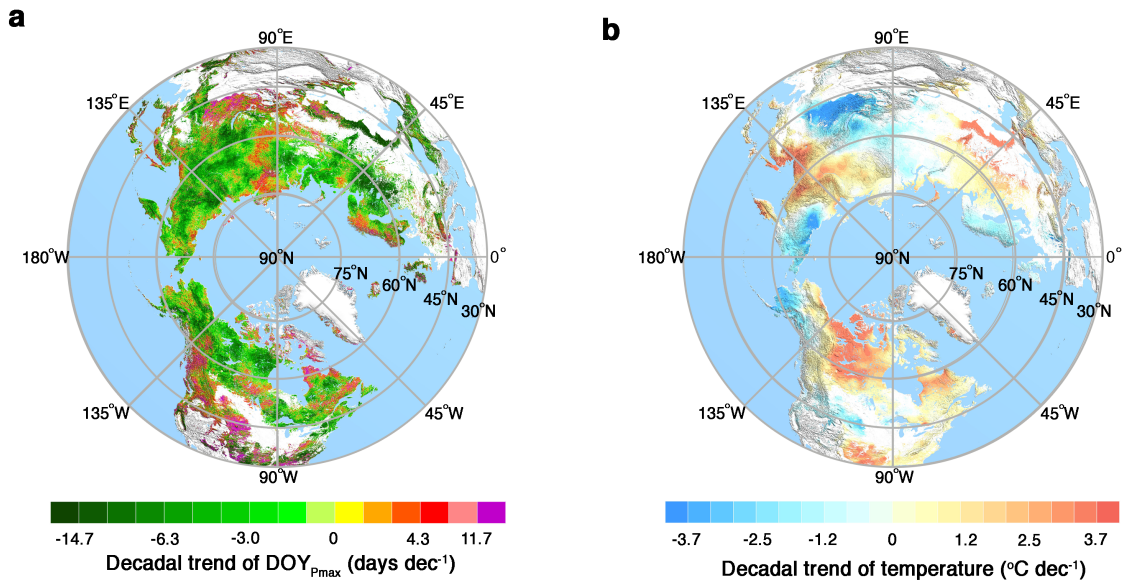

Figure 4. Spatial pattern of changes in DOY_{Pmax} and temperature during last 17 years (2000 – 2016). **a,** Decadal trend of MODIS based DOY_{Pmax} over northern land during last 17 years. **b,** Same as **a** but for summer temperature (June – August). The trend was derived based on ordinary least squares regression.

Implications of changing MODIS DOY_{Pmax} on seasonal vegetation productivity

The changes in DOY_{Pmax} have regionally varying impacts on GPP_{Total}. An 'earlier peak–larger productivity' pattern is dominant over the arctic (-0.004 ± 0.002 kg C m^{-2} day^{-1}, slope ± s.e., $P < 0.05$) and boreal (-0.006 ± 0.002 kg C m^{-2} day^{-1}, $P < 0.05$) regions under a warming climate (Figure 5c). The framework proposed earlier informs that more favorable thermal conditions enable vegetation to increase its synchrony with seasonality in incoming radiation, with the

seasonal course of photosynthetic activity tending toward the peak of radiation. Widely reported growing season extension (likely inferred from DOY_{Pmax} shift, Figure S2d) partly explains such 'earlier peak–larger productivity' relation across the arctic and boreal regions (Xu et al., 2013; Park et al., 2016). Warmer temperatures might also enhance access to key nutrients (e.g., nitrogen), thus stimulating photosynthetic rates over the course of the entire growing season (Natali et al., 2012). A weaker 'earlier peak–less productivity' pattern in the temperate regions emerges due to complex climate-vegetation interactions (Figure 5c). Here, warmer conditions without moisture-stress result in an earlier DOY_{Pmax} and larger GPP_{Pmax} and GPP_{Total}. In other parts, where moisture stress is stronger, a significant decline in both GPP_{Pmax} and GPP_{Total} is seen despite earlier DOY_{Pmax} (e.g., southwestern Eurasia) (Angert et al., 2005). In order to capture the seasonal distribution of GPP with a simple metric we evaluated the ratio (GPP_{Ratio}) of total GPP during the first half (January 1st to the long-term mean DOY_{Pmax}) to that of the whole year. We find that DOY_{Pmax} occurring one day earlier in the season increases GPP_{Ratio} by 0.28 ± 0.07 (temperate, slope ± SE, $P < 0.001$) to 0.58 ± 0.08 % (boreal, $P < 0.001$), clearly indicating an advance in gross carbon assimilation activity (Figure 5d) (Duveneck & Thompson, 2017). This is an important indicator, as the photosynthetic activity is tightly linked to the atmosphere via carbon, water and energy cycles. Thus, phase shifts in carbon, water and energy cycles could be anticipated (Richardson et al., 2013).

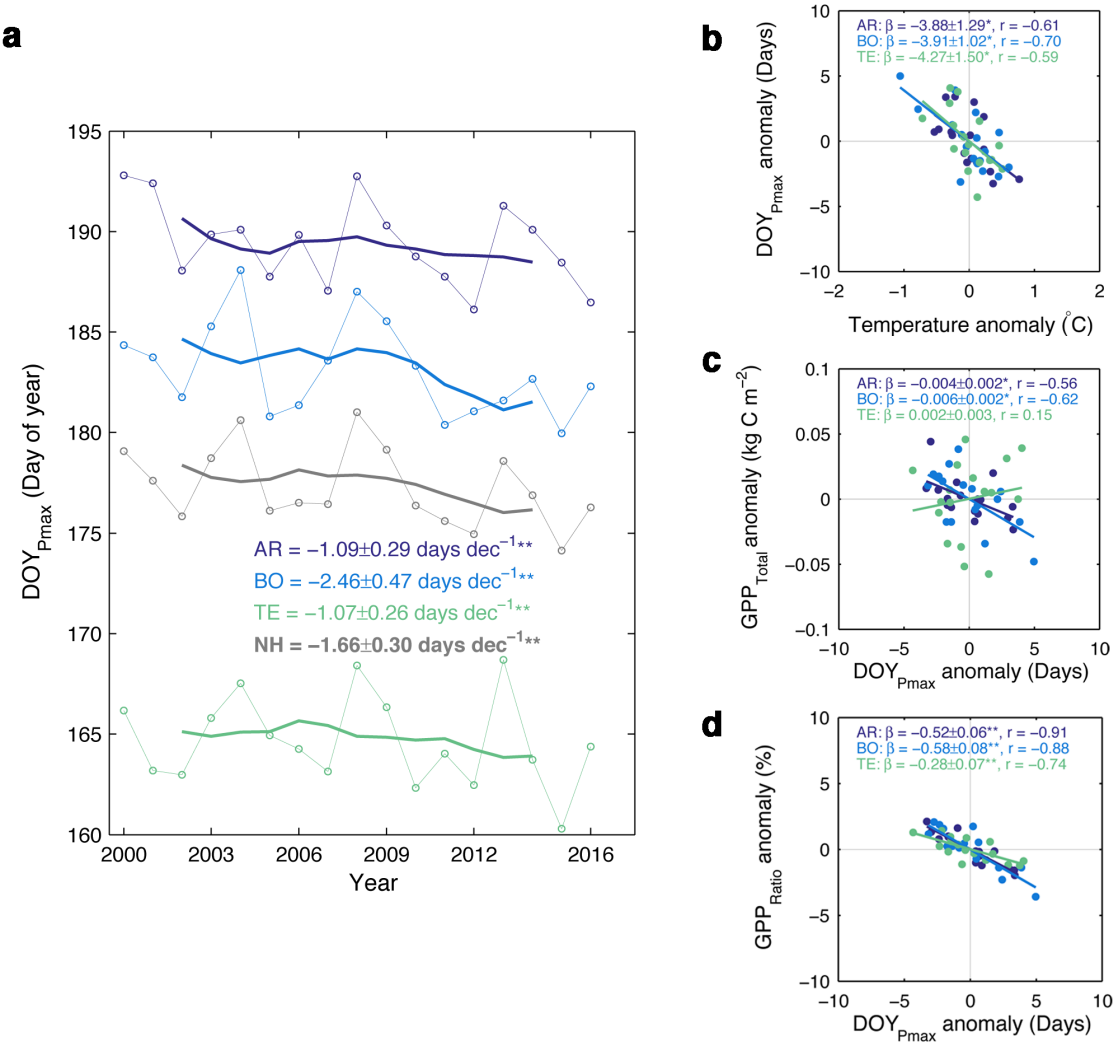

Figure 5. Changes in DOY_{Pmax} during last 17 years (2000 – 2016) and their implications on northern vegetation productivity. **a,** Inter-annual variation of DOY_{Pmax} by regions (Arctic: AR, Boreal: BO, Temperate: TE, Northern Hemisphere: NH) and its trend over last 17 years. The decadal trend is estimated based on the 5-year moving average approach to reduce the potential impact of first, last and outlier points. Thin solid line with markers and thick solid line represent annual DOY_{Pmax} and 5-year moving average. Calculated trend (slope ± SE) based on ordinary least squares regression is given with its significance level (double asterisks denote $P < 0.001$, single asterisks denote $P < 0.05$). The significance was computed by using the non-parametric Mann-Kendall trend test. **b,** Relation between regional DOY_{Pmax} and summer temperature (June – August) anomalies. **c–d,** Same as **b** but for respective relation between DOY_{Pmax} and GPP_{Total}, and DOY_{Pmax} and GPP_{Ratio} anomalies. Significance of the slope estimate (β ± SE) is denoted as double ($P < 0.001$) and single ($P < 0.05$) asterisks. The Kendall's rank correlation coefficient (r) between two variables is also given. Dark blue, light blue, green and gray stand for AR, BO, TE and NH, respectively.

Changes in phase and amplitude of CO_2 seasonal cycle

We found that earlier peak photosynthesis and more carbon assimilation in the early part of the growing season altered the seasonal course of atmospheric CO_2 concentration. We used CO_2 observations from Point Barrow and two state-of-the-art CO_2 inversion datasets (i.e., CAMS and JENA). The springtime downward CO_2 zero-crossing date ($DOY_{Zero\text{-}Crossing}$) shows trends towards earlier downward $DOY_{Zero\text{-}Crossing}$ in the three CO_2 datasets (Figure 6a). The phase of atmospheric CO_2 at Point Barrow has advanced by 1.84 ± 0.20 days decade^{-1} (slope ± SE, $P <$ 0.001) since 1972. We also observe advancing trends but steeper changes in both CAMS (−2.42 ± 0.21 days decade^{-1}, $P < 0.001$) and JENA (−3.26 ± 0.21 days decade^{-1}, $P < 0.001$). This shift corroborates the advancing DOY_{Pmax} of gross photosynthetic activity observed from space and shows the potential implications of enhanced gross carbon assimilation in the early growing season (i.e., increased GPP_{Ratio}) (Barichivich et al., 2012; Randerson et al., 1999) (Figure 5a,d). Furthermore, like as what we observed in the analysis of DOY_{Pmax} and GPP_{Total} (Figure 5c), SCA of three CO_2 data is negatively associated with $DOY_{Zero\text{-}Crossing}$ (Figure 6b). These phase shifts in the CO_2 data and their association with the enhanced seasonal amplitudes are in accordance with several observations (Barichivich et al., 2012; Randerson et al., 1999; Graven et al., 2013) and modeling studies (Duveneck & Thompson, 2017; Zhao & Zeng, 2014) suggesting enhanced peak photosynthetic activity and its advancing shift.

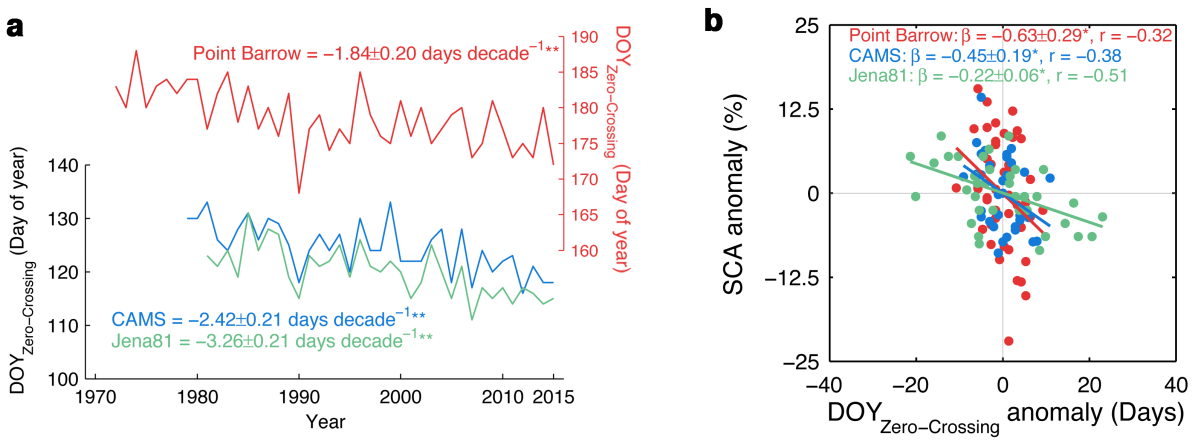

Figure 6. Analysis of atmospheric CO_2 concentration at Point Barrow and two CO_2 inversion estimates. **a,** Time series of $DOY_{Zero\text{-}Crossing}$ observed at Point Barrow atmospheric observatory and two independent CO_2 inversion datasets (CAMS and JENA). Note that the CO_2 fluxes for $DOY_{Zero\text{-}Crossing}$ retrieval of the inversion datasets are based on regionally integrated fluxes over the arctic and boreal zones, and all trend estimates are based on the 5-year moving average approach. Calculated trend (slope ± SE) based on ordinary least squares regression is given with its significance level (double asterisks denote $P < 0.001$, single asterisks denote $P < 0.05$). The significance was computed by using the non-parametric Mann-Kendall trend test. **b,** Relation between $DOY_{Zero\text{-}Crossing}$ and seasonal cycle amplitude (SCA) of atmospheric CO_2 concentration and flux estimates. SCA anomaly was expressed as percentage of long-term mean. Significance of the slope estimate (β ± SE) is denoted as double ($P < 0.001$) and single ($P < 0.05$) asterisks. The Kendall rank correlation coefficient (r) was used to measure degree of association. Red, blue, and green stand for CO_2 data from Point Barrow, CAMS, and JENA, respectively.

Changes in ESMs simulated vegetation productivity and DOY_{Pmax}

We lastly ask whether state-of-the-art terrestrial biosphere models can reproduce the observed DOY_{Pmax} changes and their consequences under historical and future climate scenarios (Figure 7). The ESMs project an advancing DOY_{Pmax} across all northern bioclimatic zones for the period 1980 to 2030. We see a pattern of regional DOY_{Pmax} trends from ESMs analogous to satellite observations, i.e. a strong trend for shifting to earlier in the season over the boreal (−0.94 ± 0.67 days decade^{-1}, mean ± 1 s.d. across all ESMs), arctic (−0.86 ± 0.71 days decade^{-1}) and temperate

464 (-0.58 ± 0.61 days decade^{-1}) regions. All models show a tightly linked negative relation between
465 DOY_{Pmax} and GPP_{Total}, revealing the 'earlier peak-larger productivity' tendency as in current
466 satellite observations. Particularly, temperature-constrained arctic and boreal regions have a
467 tighter linkage between DOY_{Pmax} and GPP_{Total} than the warmer temperate regions. The shift in
468 DOY_{Pmax} also increases the GPP_{Ratio}, indicating more carbon assimilation in the early part of the
469 growing season than in the later period (Duveneck & Thompson, 2017; Zhao & Zeng, 2014).
470 The pace of future (2050 – 2100) DOY_{Pmax} shift and its contribution to productivity is projected
471 to continue, but to be slower and weaker than at present.

472

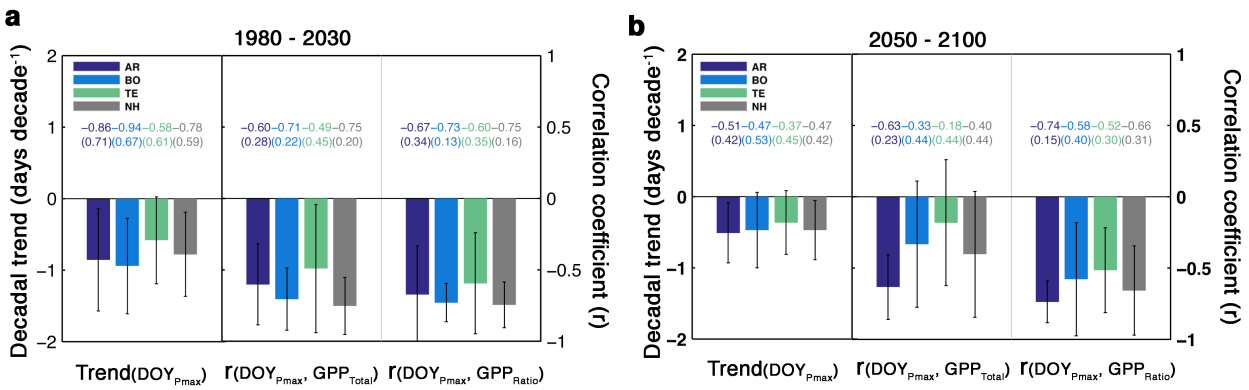

473
474 **Figure 7.** Analysis of multiple CMIP5 ESMs during two separate periods: **a,** 1980-2030 and **b,**
475 2050-2100. Decadal trend of DOY_{Pmax} (left) and its association to GPP_{Total} (center) and GPP_{Ratio}
476 (right) over northern lands inferred from the seven ESMs. Bar charts with error bars depict mean
477 ± 1 SD across all ESMs. The Kendall rank correlation coefficient (r) was used to measure degree
478 of association. Dark blue, light blue, green and gray stand for AR, BO, TE and NH, respectively.
479

480 **DISCUSSION**

481 Our analyses from long-term satellite records and ESMs reveal a widespread shift in DOY_{Pmax}
482 towards earlier in the growing season. The changes are associated with divergent consequences
483 on GPP_{Total} depending on different states of climate constraints on plant growth. For high latitude

arctic ecosystems, the advancement in DOY_{Pmax} likely continues in a warmer future climate as seen in the ESM simulations. Our framework translates the change into a continuous relaxation of temperature limit on arctic vegetation photosynthetic activity. A recent remote sensing based study supports our study by identifying a 16.4% decline in the area of vegetated land that is limited by temperature (Keenan & Riley, 2018). Yet, our framework suggests a reduction in the relative importance of temperature control on plant photosynthetic activity rather than a transitional state where other climate constraints primarily govern the ecosystem (Figure S4a). Indeed, long-term ground based studies in the Arctic tundra have shown that temperature is a primary driver of shrub growth and its expansion in arctic environment, while soil moisture controls the sensitivity of growth response to warming (Myers-Smith et al., 2015).

Some of boreal ecosystems (northwest Russia and south Fennoscandia, south and southeast Canada) show a transition from positive to negative $\delta DOY_{P,R}$ during last two decades (Figure S5). This transition does not necessarily signify a decline of GPP_{Total} because of the "phenological tradeoff" mechanism (Figure S2d). However, it is critical to monitor these ecosystems continuously because our framework suggests that there may be a tipping point where they move from temperature- towards water-limited ecosystems. That is, continuous warming and drying conditions may exacerbate moisture stress, and therefore, productivity reduction in these ecosystems. Interestingly, a recent tree-ring based study revealed that while 2 °C of warming may increase overall forest productivity, additional warming could reverse this trend and lead to substantial moisture stress (D'Orangeville et al., 2018). Also, multiple warming experiments confirm the dynamism of climate constraints on plant growth in the southern boreal

506 forest and highlight the vulnerability of the ecosystem to excess warming and drying (e.g., Reich
507 et al., 2018).
508
509 Warmer and drier conditions over temperate vegetation, where negative $\delta DOY_{P,R}$ is dominant,
510 generally result in a decrease of plant growth. Widespread increase of tree mortality of this
511 susceptible ecosystem to worsening moisture stress has been reported (Allen et al., 2010). Most
512 epidemic climate-induced tree mortality events occurs over the regions where water availability
513 is the primary climate constraint on photosynthetic activity (i.e., $\delta DOY_{P,R} < 0$, see Figure S5). It
514 agrees with the 'earlier peak–less productivity' pattern in warmer temperate vegetation from
515 MODIS data. However, the relation was not reproduced by the ESMs. The models projected that
516 warming-induced earlier peak photosynthesis leads to an enhanced seasonal total productivity
517 (Figure 7a). Recent studies have shown that current terrestrial carbon-cycle models substantially
518 overestimate (underestimate) positive (negative) effects associated with warming (Buermann et
519 al., 2018). It is possibly because these models inadequately capture the effects of the seasonal
520 build-up of water stress on seasonal vegetation growth.
521
522 Our analyses of $DOY_{zero\text{-}crossing}$ and SCA confirm the advancing and enhancing CO_2 seasonal
523 cycle in northern lands (Barichivich et al., 2012; Graven et al., 2013; Forkel et al., 2016). An
524 additional remark made here for ongoing changes in biosphere-atmosphere interaction is an
525 asymmetric enhancement of terrestrial photosynthetic activity. We find a widespread warming-
526 induced DOY_{Pmax} advancement and GPP_{Total} increase across northern lands, and these changes
527 possibly play a role in ongoing shift and amplified atmospheric CO_2 seasonal cycle. This is
528 because peak photosynthesis rate explains about 78% of the variation of seasonal total

productivity and only 21% can be explained by growing season changes (Xia et al., 2015). Our results confirm that a larger beneficial carbon uptake from an extended growing season is dominated by the later part of spring, when more fully developed leaf area with more favorable light and temperature is available for photosynthetic activity (Keenan et al., 2014). Together with these earlier studies, our findings suggest that an intra-seasonal scale may provide a possible but overlooked mechanism for the changes in atmospheric CO_2 seasonal cycle. Furthermore, the observed shift in the relative importance of climate constraints on plant growth may be a possible mechanism for the recently reported weakening temperature controls on spring carbon uptake across northern lands (Piao et al., 2017).

Furthermore, our framework also gives insight into the changes in growing season duration and its implication on carbon cycle. As described in Figure 1, thermal inertia induced decoupling of radiation and temperature characterizes a unique seasonal climate environment to local vegetation. For temperature-constrained ecosystems (see Case-2 in Figure 1), DOY_{Tmax}-ward DOY_{Pmax} positioning leads to strong temperature dependence in spring photosynthesis while light availability emerges as an important controller in autumnal activity (Garonna et al., 2018). This intrinsic physical environment indicates contrasting responses of photosynthetic activity to spring versus autumn warming. In this cold environment, spring warming generally stimulates carbon uptake by extending onset of growing season (Pulliainen et al., 2017). In contrast, autumnal growing season extension and its photosynthetic carbon gain will be strongly limited by radiation (Bauerle et al., 2012). Multiple studies have reported that the increase of autumn temperature results in net carbon loss indicating more respiratory loss than photosynthetic gain in northern lands (Piao et al., 2008; Commane et al. 2017). These contrasting seasonal responses

552 also partially explain the observed and projected asymmetric enhancement of photosynthetic
553 activity and carbon cycles in northern lands. However, further studies will be required to identify
554 which case the autumn growing season extension can lead to increased photosynthesis sufficient
555 to balance the higher respiration carbon loss.
556
557 Most of ESMs as well as MODIS GPP estimate used in this study do not include photosynthetic
558 temperature acclimation process. This physiological adjustment is commonly observed as a shift
559 in the optimum temperature for carbon assimilation rate by modulating local plant's metabolism
560 (Yamori et al., 2014). We expect that taking the photosynthetic thermal acclimation likely lead to
561 a slightly closer alignment between DOY_{Pmax} and DOY_{Rmax} than the one without the process. It
562 also may reduce the observed DOY_{Pmax} sensitivity to warming (Smith et al., 2016). Nevertheless,
563 we believe that the proposed DOY_{Pmax} framework and its changes are valid because of multiple
564 evidence from independent datasets in this work (Figures 3 and Figure S3) and previous studies
565 (Rotenberg & Yakir, 2010; Buitenwerf et al., 2015; Gonsamo et al., 2018). Interestingly,
566 dendrometer based intra-annual tree growth studies also support our framework (e.g., Rossi et
567 al., 2006). Ongoing efforts for advancements in modeling communities (Rogers et al., 2017) will
568 help to deploy temperature acclimation modules in ESMs and thus better understandings on
569 seasonal photosynthesis and DOY_{Pmax} changes are expected.
570
571 In summary, our results highlight a significant shift in terrestrial photosynthetic activity north of
572 30°N, implying a constantly adapting state of climatic constraints on plant growth. A consensus
573 of multiple Earth observations and ESMs on this change imbues confidence in our findings. This
574 is a critical development because the shifts in peak photosynthesis may cause cascading

perturbations in Earth system components that include carbon, water and energy balances (Richardson et al., 2013), as well as ecological interactions (Walther, 2010). The framework proposed here is one of the first attempts to introduce the time of peak photosynthesis as an indicator of a plant's adaptive state to climatic constraints, and provides a simplified yet realistic framework for the complex mechanisms by which various climatic factors constrain plant growth.

ACKNOWLEDGEMENTS

This work was funded by NASA Earth Science Directorate (grants NNX16AO34H, NNX14AP80A and NNX14AI71G) and the Research Council of Norway (grants 227064 and 270992). A Natural Environment Research Council Independent Research Fellowship (NE/L011859/1) funded M.M.-F.'s contribution.

AUTHOR CONTRIBUTIONS

TP and RBM designed the research; TP performed analysis and wrote the draft; and all the authors contributed to the interpretation of the results and the writing of the paper.

590 **REFERENCES**

591 Allen, C. D., Macalady, A. K., Chenchouni, H., Bachelet, D., McDowell, N., Vennetier, M., . . .
592 Hogg, E. T. (2010). A global overview of drought and heat-induced tree mortality reveals
593 emerging climate change risks for forests. Forest Ecology and Management, 259(4), 660-
594 684.

595 Angert, A., Biraud, S., Bonfils, C., Henning, C., Buermann, W., Pinzon, J., . . . Fung, I. (2005).
596 Drier summers cancel out the CO2 uptake enhancement induced by warmer springs.
597 Proceedings of the National Academy of Sciences of the United States of America, 102(31),
598 10823-10827.

599 Baldocchi, D., Falge, E., Gu, L., Olson, R., Hollinger, D., Running, S., . . . Evans, R. (2001).
600 FLUXNET: A new tool to study the temporal and spatial variability of ecosystem–scale
601 carbon dioxide, water vapor, and energy flux densities. Bulletin of the American
602 Meteorological Society, 82(11), 2415-2434.

603 Barichivich, J., Briffa, K. R., Osborn, T. J., Melvin, T. M., & Caesar, J. (2012). Thermal growing
604 season and timing of biospheric carbon uptake across the Northern Hemisphere. Global
605 Biogeochemical Cycles, 26(4).

606 Barichivich, J., Briffa, K. R., Myneni, R., Schrier, G. V. D., Dorigo, W., Tucker, C. J., ... &
607 Melvin, T. M. (2014). Temperature and snow-mediated moisture controls of summer
608 photosynthetic activity in northern terrestrial ecosystems between 1982 and 2011. Remote
609 Sensing, 6(2), 1390-1431.

610 Bauerle, W. L., Oren, R., Way, D. A., Qian, S. S., Stoy, P. C., Thornton, P. E., . . . Reynolds, R.
611 F. (2012). Photoperiodic regulation of the seasonal pattern of photosynthetic capacity and

612 the implications for carbon cycling. Proceedings of the National Academy of Sciences,
613 109(22), 8612-8617.
614 Blackman, F. F. (1905). Optima and limiting factors. Annals of botany, 19(74), 281-295.
615 Buermann, W., Forkel, M., O'Sullivan, M., Sitch, S., Friedlingstein, P., Haverd, V., ... &
616 Lombardozzi, D. (2018). Widespread seasonal compensation effects of spring warming on
617 northern plant productivity. Nature, 562(7725), 110.
618 Buitenwerf, R., Rose, L., & Higgins, S. I. (2015). Three decades of multi-dimensional change in
619 global leaf phenology. Nature Climate Change, 5(4), 364.
620 Chevallier, F., Ciais, P., Conway, T., Aalto, T., Anderson, B., Bousquet, P., . . . Fröhlich, M.
621 (2010). CO2 surface fluxes at grid point scale estimated from a global 21 year reanalysis of
622 atmospheric measurements. Journal of Geophysical Research: Atmospheres, 115(D21).
623 Chuine, I., & Beaubien, E. G. (2001). Phenology is a major determinant of tree species range.
624 Ecology Letters, 4(5), 500-510.
625 Commane, R., Lindaas, J., Benmergui, J., Luus, K.A., Chang, R.Y.W., Daube, B.C., . . . Miller,
626 S.M. (2017). Carbon dioxide sources from Alaska driven by increasing early winter
627 respiration from Arctic tundra. Proceedings of the National Academy of Sciences, 114(21),
628 5361-5366.
629 Duveneck, M. J., & Thompson, J. R. (2017). Climate change imposes phenological trade□offs
630 on forest net primary productivity. Journal of Geophysical Research: Biogeosciences,
631 122(9), 2298-2313.
632 D'Orangeville, L., Houle, D., Duchesne, L., Phillips, R. P., Bergeron, Y., & Kneeshaw, D.
633 (2018). Beneficial effects of climate warming on boreal tree growth may be transitory.
634 Nature communications, 9(1), 3213.

635 Eagleson, P. S. (2005). Ecohydrology: Darwinian expression of vegetation form and function.
636 Cambridge University Press.
637 Forkel, M., Carvalhais, N., Rödenbeck, C., Keeling, R., Heimann, M., Thonicke, K., . . .
638 Reichstein, M. (2016). Enhanced seasonal CO2 exchange caused by amplified plant
639 productivity in northern ecosystems. Science, 351(6274), 696-699.
640 Friedl, M. A., Sulla-Menashe, D., Tan, B., Schneider, A., Ramankutty, N., Sibley, A., & Huang,
641 X. (2010). MODIS Collection 5 global land cover: Algorithm refinements and
642 characterization of new datasets. Remote Sensing of Environment, 114(1), 168-182.
643 Fritz, S., See, L., McCallum, I., You, L., Bun, A., Moltchanova, E., . . . Perger, C. (2015).
644 Mapping global cropland and field size. Global Change Biology, 21(5), 1980-1992.
645 Fu, Y. H., Zhao, H., Piao, S., Peaucelle, M., Peng, S., Zhou, G., ... & Song, Y. (2015). Declining
646 global warming effects on the phenology of spring leaf unfolding. Nature, 526(7571), 104.
647 Garonna, I., de Jong, R., Stöckli, R., Schmid, B., Schenkel, D., Schimel, D., & Schaepman, M.
648 E. (2018). Shifting relative importance of climatic constraints on land surface phenology.
649 Environmental Research Letters, 13(2), 024025.
650 Gelaro, R., McCarty, W., Suárez, M. J., Todling, R., Molod, A., Takacs, L., ... & Wargan, K.
651 (2017). The modern-era retrospective analysis for research and applications, version 2
652 (MERRA-2). Journal of Climate, 30(14), 5419-5454.
653 Gonsamo, A., Chen, J. M., & Ooi, Y. W. (2018). Peak season plant activity shift towards spring
654 is reflected by increasing carbon uptake by extratropical ecosystems. Global change biology,
655 24(5), 2117-2128.

656 Graven, H. D., Keeling, R. F., Piper, S. C., Patra, P. K., Stephens, B. B., Wofsy, S. C., ... &
657 Daube, B. C. (2013). Enhanced seasonal exchange of CO2 by northern ecosystems since
658 1960. Science, 1239207.

659 Heinsch, F. A., Zhao, M., Running, S. W., Kimball, J. S., Nemani, R. R., Davis, K. J., . . .
660 Ricciuto, D. M. (2006). Evaluation of remote sensing based terrestrial productivity from
661 MODIS using regional tower eddy flux network observations. IEEE Transactions on
662 Geoscience and Remote Sensing, 44(7), 1908-1925.

663 Ito, A., Inatomi, M., Huntzinger, D. N., Schwalm, C., Michalak, A. M., Cook, R., . . . Post, W.
664 M. (2016). Decadal trends in the seasonal-cycle amplitude of terrestrial CO2 exchange
665 resulting from the ensemble of terrestrial biosphere models. Tellus B: Chemical and
666 Physical Meteorology, 68(1), 28968.

667 Joiner, J., Yoshida, Y., Guanter, L., & Middleton, E. M. (2016). New methods for the retrieval of
668 chlorophyll red fluorescence from hyperspectral satellite instruments: simulations and
669 application to GOME-2 and SCIAMACHY. Atmospheric Measurement Techniques, 9(8).

670 Jolly, W. M., Nemani, R., & Running, S. W. (2005). A generalized, bioclimatic index to predict
671 foliar phenology in response to climate. Global Change Biology, 11(4), 619-632.

672 Keenan, T. F., Gray, J., Friedl, M. A., Toomey, M., Bohrer, G., Hollinger, D. Y., . . . Wing, I. S.
673 (2014). Net carbon uptake has increased through warming-induced changes in temperate
674 forest phenology. Nature Climate Change, 4(7), 598-604.

675 Keenan, T., & Riley, W. (2018). Greening of the land surface in the world's cold regions
676 consistent with recent warming. Nature Climate Change, 8(9), 825.

677 Lasslop, G., Reichstein, M., Papale, D., Richardson, A. D., Arneth, A., Barr, A., . . . Wohlfahrt,
678 G. (2010). Separation of net ecosystem exchange into assimilation and respiration using a

679 light response curve approach: critical issues and global evaluation. Global Change Biology,
680 16(1), 187-208.
681 Liebig, J. (1841). Organic chemistry in its applications to agriculture and physiology. J. Owen.
682 Myers-Smith, I. H., Elmendorf, S. C., Beck, P. S., Wilmking, M., Hallinger, M., Blok, D., ... &
683 Speed, J. D. (2015). Climate sensitivity of shrub growth across the tundra biome. Nature
684 Climate Change, 5(9), 887.
685 Natali, S. M., Schuur, E. A., & Rubin, R. L. (2012). Increased plant productivity in Alaskan
686 tundra as a result of experimental warming of soil and permafrost. Journal of Ecology,
687 100(2), 488-498.
688 Nemani, R. R., Keeling, C. D., Hashimoto, H., Jolly, W. M., Piper, S. C., Tucker, C. J., . . .
689 Running, S. W. (2003). Climate-driven increases in global terrestrial net primary production
690 from 1982 to 1999. Science, 300(5625), 1560-1563.
691 Olson, D. M., Dinerstein, E., Wikramanayake, E. D., Burgess, N. D., Powell, G. V., Underwood,
692 E. C., . . . Morrison, J. C. (2001). Terrestrial Ecoregions of the World: A New Map of Life
693 on Earth: A new global map of terrestrial ecoregions provides an innovative tool for
694 conserving biodiversity. Bioscience, 51(11), 933-938.
695 Park, T., Ganguly, S., Tømmervik, H., Euskirchen, E. S., Høgda, K.-A., Karlsen, S. R., . . .
696 Myneni, R. B. (2016). Changes in growing season duration and productivity of northern
697 vegetation inferred from long-term remote sensing data. Environmental Research Letters,
698 11(8), 084001.
699 Parmesan, C., & Yohe, G. (2003). A globally coherent fingerprint of climate change impacts
700 across natural systems. Nature, 421(6918), 37.

Pastorello, G., Papale, D., Chu, H., Trotta, C., Agarwal, D., Canfora, E., ... & Torn, M. (2017). A new data set to keep a sharper eye on land-air exchanges. Eos, Transactions American Geophysical Union (Online), 98(8).

Peng, C., Ma, Z., Lei, X., Zhu, Q., Chen, H., Wang, W., ... & Zhou, X. (2011). A drought-induced pervasive increase in tree mortality across Canada's boreal forests. Nature climate change, 1(9), 467.

Piao, S., Ciais, P., Friedlingstein, P., Peylin, P., Reichstein, M., Luyssaert, S., . . . Chen, A. (2008). Net carbon dioxide losses of northern ecosystems in response to autumn warming. Nature, 451(7174), 49-52.

Piao, S., Liu, Z., Wang, T., Peng, S., Ciais, P., Huang, M., . . . Janssens, I. A. (2017). Weakening temperature control on the interannual variations of spring carbon uptake across northern lands. Nature Climate Change, 7(5), 359-363.

Prentice, I. C., Cramer, W., Harrison, S. P., Leemans, R., Monserud, R. A., & Solomon, A. M. (1992). Special paper: a global biome model based on plant physiology and dominance, soil properties and climate. Journal of Biogeography, 117-134.

Pulliainen, J., Aurela, M., Laurila, T., Aalto, T., Takala, M., Salminen, M., . . . Laaksonen, A. (2017). Early snowmelt significantly enhances boreal springtime carbon uptake. Proceedings of the National Academy of Sciences, 114(42), 11081-11086.

Randerson, J., Field, C., Fung, I., & Tans, P. (1999). Increases in early season ecosystem uptake explain recent changes in the seasonal cycle of atmospheric CO2 at high northern latitudes. Geophysical Research Letters, 26(17), 2765-2768.

722 Reich, P. B., Sendall, K. M., Stefanski, A., Rich, R. L., Hobbie, S. E., & Montgomery, R. A.
723 (2018). Effects of climate warming on photosynthesis in boreal tree species depend on soil
724 moisture. Nature, 562(7726), 263.
725 Richardson, A. D., Black, T. A., Ciais, P., Delbart, N., Friedl, M. A., Gobron, N., ... &
726 Migliavacca, M. (2010). Influence of spring and autumn phenological transitions on forest
727 ecosystem productivity. Philosophical Transactions of the Royal Society of London B:
728 Biological Sciences, 365(1555), 3227-3246.
729 Richardson, A. D., Keenan, T. F., Migliavacca, M., Ryu, Y., Sonnentag, O., & Toomey, M.
730 (2013). Climate change, phenology, and phenological control of vegetation feedbacks to the
731 climate system. Agricultural and Forest Meteorology, 169, 156-173.
732 Rodell, M., Houser, P., Jambor, U., Gottschalck, J., Mitchell, K., Meng, C., . . . Bosilovich, M.
733 (2004). The global land data assimilation system. Bulletin of the American Meteorological
734 Society, 85(3), 381-394.
735 Rödenbeck, C., Houweling, S., Gloor, M., & Heimann, M. (2003). CO 2 flux history 1982–2001
736 inferred from atmospheric data using a global inversion of atmospheric transport.
737 Atmospheric Chemistry and Physics, 3(6), 1919-1964.
738 Rogers, A., Medlyn, B.E., Dukes, J.S., Bonan, G., Von Caemmerer, S., Dietze, M.C., . . .
739 Prentice, I.C. (2017). A roadmap for improving the representation of photosynthesis in Earth
740 system models. New Phytologist, 213(1), 22-42.
741 Rossi, S., Deslauriers, A., Anfodillo, T., Morin, H., Saracino, A., Motta, R., . . . Borghetti, M.
742 (2006). Conifers in cold environments synchronize maximum growth rate of tree-ring
743 formation with day length. New phytologist, 170(2), 301-310.

744 Rotenberg, E., & Yakir, D. (2010). Contribution of semi-arid forests to the climate system.
745 Science, 327(5964), 451-454.
746 Running, S., Mu, Q., & Zhao, M. (2015). MOD17A2H MODIS/Terra Gross Primary
747 Productivity 8-Day L4 Global 500m SIN Grid V006. NASA EOSDIS Land Processes
748 DAAC.
749 Smith, N.G., Malyshev, S.L., Shevliakova, E., Kattge, J., & Dukes, J.S. (2016). Foliar
750 temperature acclimation reduces simulated carbon sensitivity to climate. Nature Climate
751 Change, 6(4), 407.
752 Sprengel, C. (1828). Von den Substanzen der Ackerkrume und des Untergrundes (About the
753 substances in the plow layer and the subsoil). Journal for Technische and Okonomische
754 Chemie, 2, 397-421.
755 Taylor, K. E., Stouffer, R. J., & Meehl, G. A. (2012). An overview of CMIP5 and the experiment
756 design. Bulletin of the American Meteorological Society, 93(4), 485-498.
757 Thomson, A. M., Calvin, K. V., Smith, S. J., Kyle, G. P., Volke, A., Patel, P., . . . Clarke, L. E.
758 (2011). RCP4. 5: a pathway for stabilization of radiative forcing by 2100. Climatic Change,
759 109(1-2), 77.
760 Thoning, K. W., Tans, P. P., & Komhyr, W. D. (1989). Atmospheric carbon dioxide at Mauna
761 Loa Observatory: 2. Analysis of the NOAA GMCC data, 1974–1985. Journal of
762 Geophysical Research: Atmospheres, 94(D6), 8549-8565.
763 Vautard, R., Yiou, P., & Ghil, M. (1992). Singular-spectrum analysis: A toolkit for short, noisy
764 chaotic signals. Physica D: Nonlinear Phenomena, 58(1-4), 95-126.

765 Walther, G. R. (2010). Community and ecosystem responses to recent climate change.
766 Philosophical Transactions of the Royal Society of London B: Biological Sciences,
767 365(1549), 2019-2024.

768 Welp, L. R., Patra, P. K., Rödenbeck, C., Nemani, R., Bi, J., Piper, S. C., & Keeling, R. F.
769 (2016). Increasing summer net CO 2 uptake in high northern ecosystems inferred from
770 atmospheric inversions and comparisons to remote-sensing NDVI. Atmospheric Chemistry
771 and Physics, 16(14), 9047-9066.

772 Xia, J., Niu, S., Ciais, P., Janssens, I. A., Chen, J., Ammann, C., . . . Bonal, D. (2015). Joint
773 control of terrestrial gross primary productivity by plant phenology and physiology.
774 Proceedings of the National Academy of Sciences, 112(9), 2788-2793.

775 Xu, L., Myneni, R., Chapin Iii, F., Callaghan, T., Pinzon, J., Tucker, C., . . . Tømmervik, H.
776 (2013). Temperature and vegetation seasonality diminishment over northern lands. Nature
777 Climate Change, 3(6), 581-586.

778 Yamori, W., Hikosaka, K., & Way, D.A. (2014). Temperature response of photosynthesis in C3,
779 C4, and CAM plants: temperature acclimation and temperature adaptation. Photosynthesis
780 research, 119(1-2), 101-117.

781 Zhang, Y., Guanter, L., Berry, J. A., Joiner, J., van der Tol, C., Huete, A., ... & Köhler, P. (2014).
782 Estimation of vegetation photosynthetic capacity from space-based measurements of
783 chlorophyll fluorescence for terrestrial biosphere models. Global Change Biology, 20(12),
784 3727-3742.

785 Zhao, F., & Zeng, N. (2014). Continued increase in atmospheric CO 2 seasonal amplitude in the
786 21st century projected by the CMIP5 Earth system models. Earth System Dynamics, 5(2),
787 423.

788 Zhao, M., Heinsch, F. A., Nemani, R. R., & Running, S. W. (2005). Improvements of the
789 MODIS terrestrial gross and net primary production global data set. Remote Sensing of
790 Environment, 95(2), 164-176.
791 Zhou, S., Zhang, Y., Ciais, P., Xiao, X., Luo, Y., Caylor, K. K., ... & Wang, G. (2017).
792 Dominant role of plant physiology in trend and variability of gross primary productivity in
793 North America. Scientific Reports, 7, 41366.